Int. J. Solids Structures Vol. 29, No. 24, pp. 3269–3288, 1992
Printed in Great Britain.

0020–7683/92 $5.00 + .00

ALEXANDER REVISITED—A TWO FOLDING ELEMENTS MODEL OF PROGRESSIVE CRUSHING OF TUBES

T. WIERZBICKI
Department of Ocean Engineering, M.I.T., Cambridge, MA 02139, U.S.A.

S. U. BHAT
Amoco Production Company, Tulsa, OK, U.S.A.

W. ABRAMOWICZ
Center for Transportation Studies, M.I.T., Cambridge, MA 02139, U.S.A.

and

D. BRODKIN
Ove Arup and Partners, New York, NY, U.S.A.

(*Received* 18 *April* 1991; *in revised form* 23 *April* 1992)

Abstract—A new model of the progressive crushing of circular tubes is developed in which an active zone of plastic deformations contains two folds or buckles. The model captures, with great realism, several features of the crushing process which were unaccounted for in all previous computational models of progressive folding. These include: finite values of the load peaks, alternating heights of the peaks, unequal distances between peaks, reduced crush distance, realistic final shape of crushed tubes and a longer distance between the two first peaks.

Closed-form solutions, derived for the length of the plastic folding wave and the mean crushing force, show very good agreement with experimental results. The history of the crushing force is shown to depend on the eccentricity parameter, i.e. on the way the tube material folds with respect to the original tube radius. However, the mean crushing force is found to be independent of the eccentricity parameter.

1. INTRODUCTION

Thin walled prismatic columns made of a ductile material, when subjected to an axial load, collapse either in symmetrical buckles (such as concertina modes in thick tubes) or in a non-symmetric (diamond) pattern. A typical force–axial displacement characteristic of a column is shown in Fig. 1. Apart from the initial peak, which is governed by elastic–plastic buckling, the load–displacement behavior exhibits a repeated pattern. Each pair of peaks is associated with the development of one full wrinkle or buckle. Usually, the buckles develop sequentially from one end of the tube so that the phenomenon is known as progressive crushing. Furthermore, except for very thick tubes, there is an alternating pattern of higher and lower peaks. Each point on the load–deflection diagram corresponds to a certain stage of the folding process. The area under the curve between two points representing one complete deformation cycle δ_{eff} is proportional to the so-called mean crushing force P_{m}.

Early theoretical work on the plastic collapse of tubes and columns (Alexander, 1960; Pugsley and Macaulay, 1960; Pugsley, 1979; Soden *et al.*, 1974) was based on the final, deformed shape of the crushed structures without considering the effect of the loading paths. A close examination of instantaneous deformed shapes of tubes reveals that crushing is a continuous process and that the material constantly flows in and out of the plastically deforming zone. The correspondence between the changing geometry of the collapsing tube and the resulting crushing force was studied experimentally by, among others, Johnson *et al.* (1977) and more recently by Jones (1989). Although a number of interesting observations were made, no modifications to the generally accepted computational model of the shell were suggested.

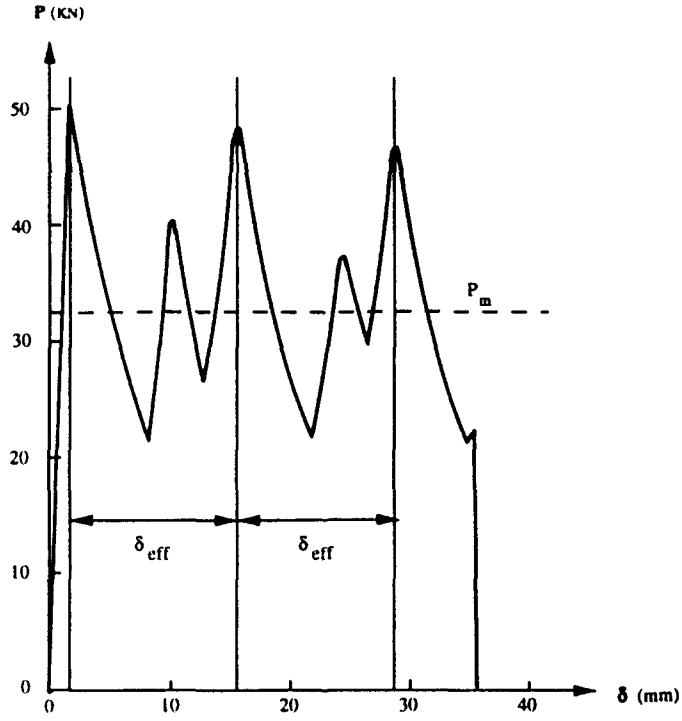

Fig. 1. Experimental static axial load versus crushing distance showing unequal magnitude of load peaks and unequal distance between subsequent peaks.

Meanwhile, a different direction of research was pursued by the present authors. Rather than continuing with experimentation in which it is difficult to control the local processes of folding, internal contacts, etc., a specialized computer graphics program, called VISTA, was developed to illustrate a column during any stage of progressive crushing (Brodkin, 1988). VISTA translates the basic kinematic assumptions of the individual folding mechanisms into precise visual images. We have used VISTA to critically assess the assumptions underlying existing crash models and test alternative sequences of folding modes.

This research has led to the development of a new computational model of progressive crushing of prismatic columns and cylinders based on the assumption that an active crush zone (or transition zone) comprises *two folding waves*. This model eliminates all the drawbacks of the existing models and is capable of reproducing qualitatively and quantitatively the main features of the experimental load–deflection diagram, as shown in Fig. 1. Among these features is the finite magnitude of the local peaks, the alternating character of the lower and higher peaks and a realistic final shape of the deformed tube.

The new modeling concept is quite general and applies to rectangular and square prismatic columns as well as circular tubes. However, for the sake of illustration and derivation of simple closed-form solutions, we chose in the present paper a circular tube collapsing in an axisymmetric or concertina mode (see Fig. 2). This brings us to the famous work by Alexander.

2. LIMITATIONS OF ALEXANDER'S SOLUTION

A first theoretical analysis of the plastic collapse of a cylindrical shell under axial load was presented by Alexander (1960). He derived a simple expression for the mean crushing force and the length of the plastic folding wave by considering two separate plastic dissipation mechanisms: axial bending in concentrated hinge lines and circumferential stretching of the shell material between the hinge lines. The main kinematic assumption made by Alexander was that *one fold was formed at a time*. It was further assumed that a given element goes through the entire crushing process before its neighbor begins to deform. After the element is crushed, the tube returns to its ultimate compressive capacity at the

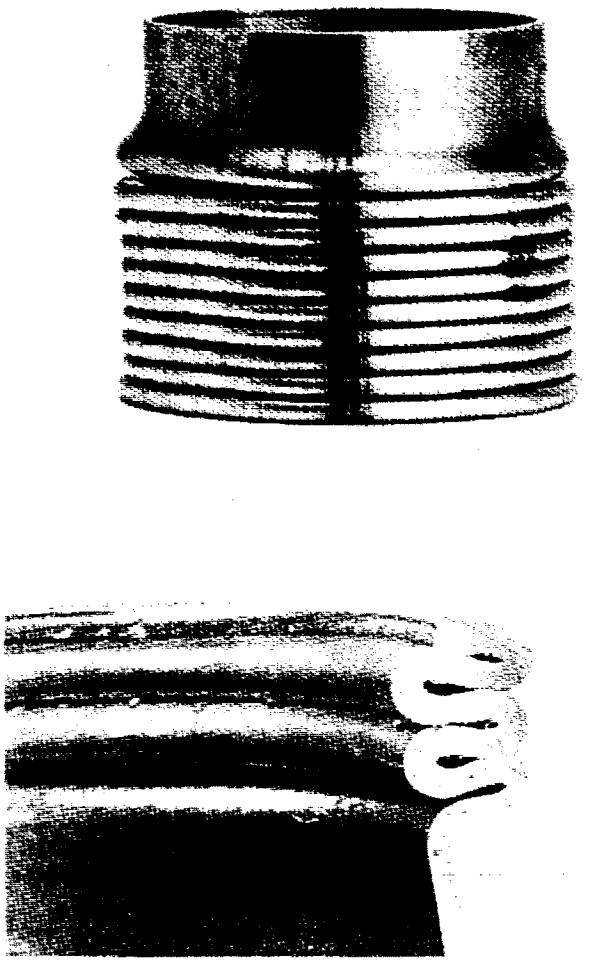

Fig. 2. Photograph showing the axisymmetric (or concertina) deformation mode in a partially crushed tube.

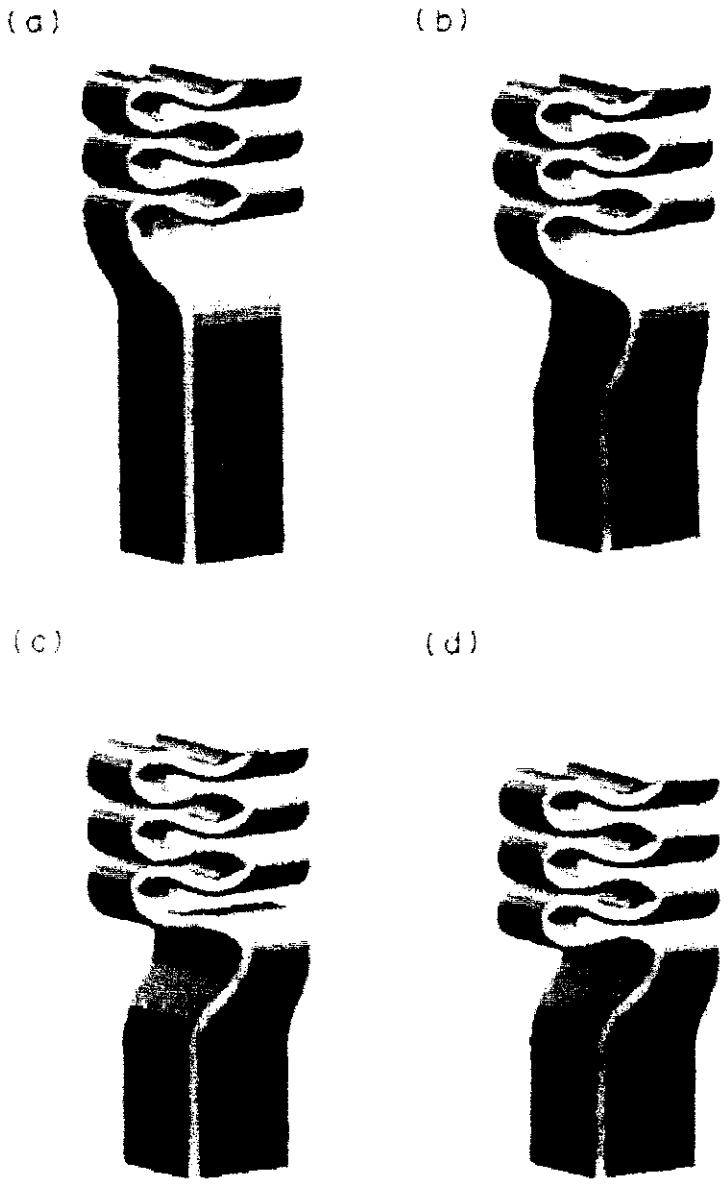

Fig. 14. Images generated by VISTA demonstrate the crushing of the two-element transition zone model in the square prismatic tube.

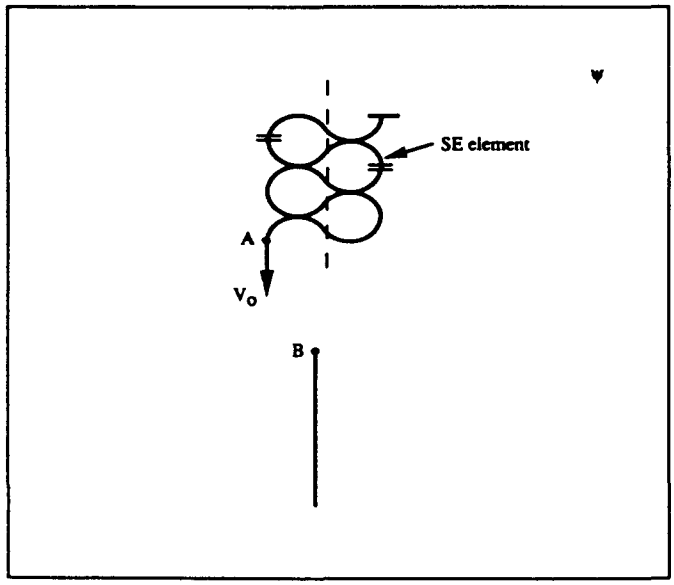

Fig. 3. Basic requirements of a transition zone between an already crushed and an undeformed part of the tube.

end of each cycle; a characteristic which is not observed experimentally. Furthermore, in the model with stationary plastic hinges, a cylindrical shell is deformed into a system of flat annular discs meaning that the entire length of the tube is available for crushing. This result is grossly inaccurate for a plastic work hardening material and gives an unrealistic final shape of the tube. Also, the amount of energy absorbed per unit crush distance or per one fold was underestimated in Alexander's solution by some 40%.

Despite its various limitations, the assumption that one folding wave forms at a time has remained unchallenged until the present time. Alexander's formulation, with only minor modification (Abramowicz and Jones, 1986), has formed the basis for crush calculations for over 30 years. A comparison of various existing calculation methods was recently presented by Grzebieta and Murray (1989). The approach developed for circular tubes was later extended to rectangular tubes (Abramowicz and Wierzbicki, 1989).

Wierzbicki and Bhat (1986) modified Alexander's solution and replaced stationary plastic hinges with moving hinges. This led to a realistic deformed shape and improved prediction of the mean crushing force. However, because the main simplifying assumption that one folding wave forms at a time remained unchanged, the modified model retained the unrealistic features of Alexander's solution.

The original analysis developed by Alexander was motivated by a specific need for predicting energy absorption of tubes subjected to dropped objects in nuclear reactor applications. Interestingly, much of the current industrial research effort is driven by similar practical needs (Magee and Thornton, 1978; Mahmood *et al.*, 1986). An enormous amount of empirical knowledge has been accumulated to date on the strength and energy absorption of tubes in terms of geometry, material properties and loading conditions (Jones, 1989). Parallel to experimental efforts, several specialized FE codes for crashworthiness applications such as PAM-CRASH (Haug *et al.*, 1986) and DYNA-3D (Hallquist and Benson, 1986) can now reproduce with some realism the actual crushing process.

Despite all these advances, a full understanding of the physics of the problem is lacking or lags behind practical applications. Alexander proposed a simple technique for estimating the global parameters of the crushing process such as a mean crushing force and the energy absorbed by compressed members. The present paper makes a further important step in this direction by providing a basis for reproducing the entire crushing process of thin-walled columns under compressive loading.

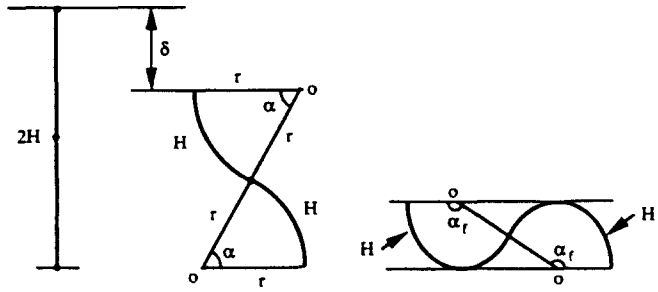

Fig. 4. Undeformed, partially deformed and fully crushed individual superfolding element.

3. MODELING THE TRANSITION ZONE

In this section, we present the basic concept of the Superfolding Element (SE) and the transition zone model. Consider a cross-section of a circular tube of initial radius R_0 and thickness t collapsing in the axisymmetric or concertina model. It is assumed that the crushed part of the tube is composed of alternating, densely packed circles. The undeformed part of the tube is straight. Figure 3 illustrates the basic requirements of the transition zone of plastic deformation between the densely packed circles and straight tube in our simplified representation. We must connect point A of the already crushed tube with point B of the undeformed zone. Point A is assumed to move vertically with a constant velocity to simulate the crushing process. Point B is stationary until a new contact between the lobes occurs. Our task is accomplished in three steps.

First, we identify a representative element of the crushed zone from which the entire deformed tube can be assembled by translation, rotation and mirror reflection. Such an element, referred to as a *Superfolding Element*, is isolated from the tube by two horizontal cuts shown in Fig. 4. Thus, symmetry rather than boundary conditions are used to generate the SE. This represents a radical departure from the current practice of developing simplified models for crushing.

In the second step we represent the various deformation stages of the SE by varying an angle α (Fig. 4). Note that the length of the SE is constant and equal to $2H$. The span, the height and the circular arc radii of the SE are uniquely determined by α and $2H$.

Finally, it is observed that the kinematic requirements of the transition zone are satisfied by two SEs. Thus, a transition zone can be formed in a unique and elegant way by connecting two "S" curves (Superfolding Elements) in series.

Figure 5 demonstrates the crushing of the two-element model in our new representation. Note that after element 1 is completely crushed so that touching occurs, the transition zone shifts downward by one SE and the process is repeated with participating elements 2 and

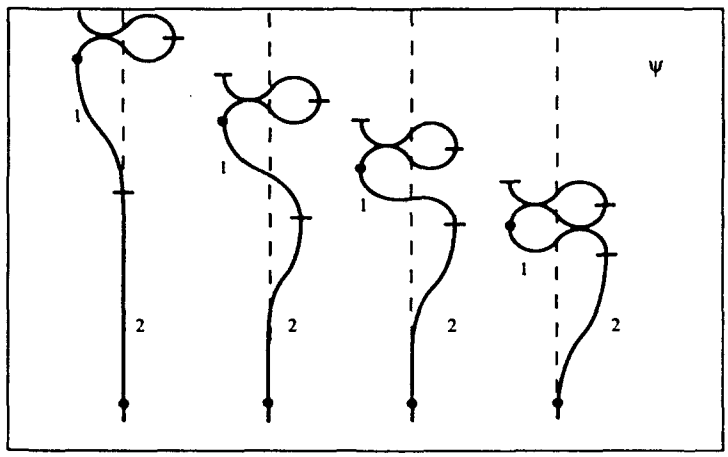

Fig. 5. Subsequent deformation stages of the two-element model.

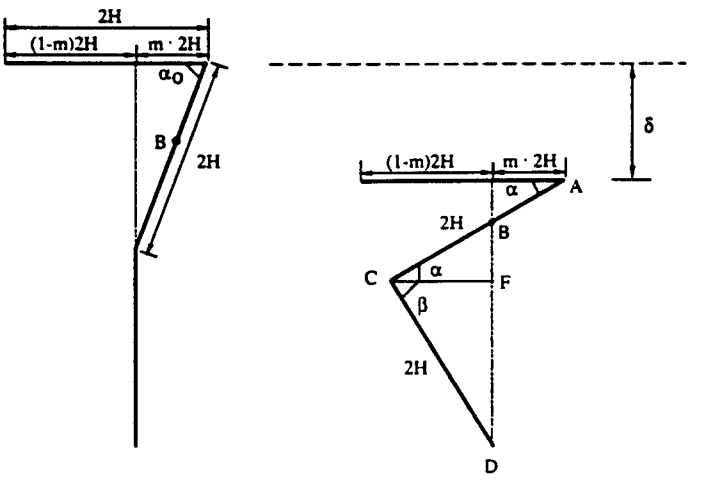

Fig. 6. A transition zone consisting of two superfolding elements.

3. The two element transition zone is relatively simple and represents the geometry of actual columns quite closely. An additional unique feature of the assumed kinematics is that the amount of inside and outside folding does not have to be the same, as explained in the next two sections. Before the present model is used to predict the load-shortening characteristics of the crushed tube, a simplified version of this model will be analysed to highlight some important features of the modeling concept.

4. MODEL WITH STATIONARY HINGES

Consider first a model of the transition zone consisting of two straight elements of length $2H$ each. The elements are connected by stationary plastic hinges. Note that straight segments in the cross-sectional plane correspond in reality to truncated cones while plastic hinges are in fact circular hinge lines (Fig. 6). Experiments show that the material folds to both sides of the original radius of the cylinder. The eccentricity of the folding process is conveniently described by the parameter m. For $m = 0.5$ the folds extend the same distance on both sides of the initial radius. A fully external folding corresponds to $m = 0$ while an internal folding is obtained by setting $m = 1$. The wavelength H is an unknown parameter which will be found in the course of the analysis. At the same time, the eccentricity parameter must be assumed.

Geometry

It is convenient to take as a reference configuration an inclination angle of the first element α_0 (ABC) such that the next element (CD) is positioned vertically. The eccentricity parameter is related to the angle α_0 by

$$\cos \alpha_0 = m. \tag{1}$$

Throughout the folding process, the inclination of the first deforming element, ABC, with respect to the horizontal is denoted by α. The second element CD is inclined by the angle β. From the geometry of the problem, the angles α and β are related by

$$\cos \beta = \cos \alpha - \cos \alpha_0, \tag{2}$$

and their rates obey

$$\dot{\beta} = \sin \alpha [1 - (\cos \alpha - \cos \alpha_0)^2]^{-1/2} \dot{\alpha}. \tag{3}$$

Therefore, the present two-element folding mechanism represents a one-degree-of-freedom

system with α as a process parameter. The shortening of the column δ, measured from the reference position can be calculated from (see Fig. 6)

$$\delta = 2H(1+\sin\alpha_0-\sin\alpha-\sin\beta), \tag{4}$$

and its rate is related to $\dot{\alpha}$ by

$$\dot{\delta} = -2H[\dot{\alpha}\cos\alpha+\dot{\beta}\cos\beta]. \tag{5}$$

Bending energy

The rate of bending energy, $\dot{E}_b$, is defined by

$$\dot{E}_b = \sum_i 2\pi R_0 M_0|\dot{\theta}_i|, \tag{6}$$

where $M_0 = 1/4\sigma_0 h^2$ is the fully plastic bending moment per unit length and σ_0 is a flow stress of the material. The relative rate of rotation in the ith plastic hinge is denoted by $\dot{\theta}_i$.

In the present two-fold model there are three active hinge circles at any time. The relative rates of rotation at these hinges are:

$$\begin{aligned}\dot{\theta}_1 &= \dot{\alpha},\\ \dot{\theta}_2 &= \dot{\alpha}+\dot{\beta},\\ \dot{\theta}_3 &= -\dot{\beta}.\end{aligned} \tag{7}$$

The rate of bending energy in the tube becomes

$$\dot{E}_b = 4\pi R_0 M_0(|\dot{\alpha}|+|\dot{\beta}|). \tag{8}$$

The bending energy is obtained by integrating $\dot{E}_b$ with respect to time over the duration of the folding cycle 0–t_f:

$$E_b = \int_0^{t_f} \dot{E}_b \, dt. \tag{9}$$

The total folding cycle corresponds to a crush distance of $4H$. During the first half of the cycle the angle α changes from α_0 to 0, until touching of the first element occurs. During the second half of the cycle the angle β changes from β_0 to 0. Now, consider the first half cycle and replace the integration with respect to time by integration with respect to the rotation angle α:

$$E_b^I = \int_{\alpha_0}^{0} \dot{E}_b \, d\alpha. \tag{10}$$

Substituting eqn (8) into eqn (10) and performing calculations one gets

$$E_b^I = 4\pi R_0 M_0\left[\frac{\pi}{2}+\cos^{-1} m-\cos^{-1}(1-m)\right]. \tag{11}$$

During the next half cycle m becomes $1-m$. Therefore,

$$E_b^{II} = 4\pi R_0 M_0 \left[\frac{\pi}{2} + \cos^{-1}(1-m) - \cos^{-1} m\right]. \tag{12}$$

The total bending energy over the crush distance of $4H$ is

$$E_b = E_b^{I} + E_b^{II} = 4\pi^2 M_0 R_0. \tag{13}$$

Thus, E_b is seen to be independent of the parameter m.

Membrane energy

The membrane energy results from compression or extension of a shell element in the hoop direction

$$\dot{E}_m = \int_S |N_0 \dot{\varepsilon}_{\theta\theta}| \, dS, \tag{14}$$

where $N_0 = \sigma_0 h$ is the fully plastic membrane force per unit length. Note that no interaction is assumed between bending moment and membrane force. The circumferential strain rate is defined as

$$\dot{\varepsilon}_{\theta\theta} = \frac{\dot{w}}{R_0}, \tag{15}$$

where $\dot{w}$ is the radial velocity of material points. The contribution of the axial components to the rate of membrane energy vanishes in view of the assumed inextensibility of the shell elements ($\dot{\varepsilon}_{xx} = 0$) and the shearing strain rate is zero because the problem is axisymmetric. The integration in eqn (14) is performed over the active zone of plastic deformation, $ds_0 = 2\pi R_0 \, ds$. Thus

$$\dot{E}_m = 2\pi R_0 N_0 \int_{ABCD} \left|\frac{\dot{w}(s)}{R_0}\right| ds, \tag{16}$$

where s is the coordinate measured along the deforming element ABCD (see Fig. 6). The expressions for $w(s)$ and $\dot{w}(s)$ in the deforming regions are given in Appendix A. Introducing eqn (A1) into eqn (10) and integrating over the length parameter S in the first half of the cycle, one gets

$$\dot{E}_m^{I} = -8\pi N_0 H^2 \sin\alpha \, \dot{\alpha}. \tag{17}$$

Note that in the first half of the loading cycle $\dot{w}(s) > 0$ and $\dot{\varepsilon}(s) > 0$. Thus, all material points are subjected to tension. The membrane energy is obtained by integrating $\dot{E}_m$ with respect to time:

$$E_m^{I} = \int_0^{t_1} \dot{E}_m^{I} \, dt = \int_{\alpha_0}^{0} \dot{E}_m^{I}(\alpha) \, d\alpha. \tag{18}$$

Introducing eqn (17) into eqn (18), the membrane energy over the first half cycle is

$$E_m^{I} = 8\pi N_0 H^2 (1-m). \tag{19}$$

In the second half cycle, all material points are moving inwards, meaning compressive loading. The membrane energy is obtained by replacing $(1-m)$ by m:

$$E_m = 8\pi N_0 H^2 m. \tag{20}$$

Thus, the total membrane energy over the entire loading cycle of the length $4H$ is

$$E_m = E_m^{I} + E_m^{II} = 8\pi N_0 H^2. \tag{21}$$

The mean crushing force P_m is defined by the global energy balance

$$P_m 4H = E_b + E_m. \tag{22}$$

Substituting eqns (13) and (21) into eqn (22), the normalized mean crushing force becomes

$$\frac{P_m}{M_0} = \frac{8\pi}{h} H + \frac{\pi^2 R}{H}. \tag{23}$$

Following Alexander, it is postulated that the half length of the folding wave adjusts itself so as to minimize the mean crushing force. Indeed, an analytical minimum of the right-hand side of eqn (23) with respect to H exists and occurs at

$$\frac{H}{R_0} = \sqrt{\frac{\pi}{4}} \sqrt{\frac{h}{2R_0}} \cong 0.886 \sqrt{\frac{h}{2R_0}}. \tag{24}$$

Further justification of the minimum condition can be found in Jones (1989). Substituting the above result back into eqn (23), the optimum value for the mean crushing force is given by the following expression:

$$\frac{P_m}{M_0} = 4\pi^{3/2} \sqrt{\frac{2R_0}{h}} \cong 22.27 \sqrt{\frac{2R_0}{h}}. \tag{25}$$

The above solution compares favorably with a similar formula derived by Alexander in which the numerical coefficient was 20.73.

The main conclusion from that part of the analysis is that the mean crushing force does not depend on the eccentricity parameter m. Furthermore, there is a strain reversal during the complete loading cycle.

The load-shortening behavior

The instantaneous equilibrium of the tube in the transition zone can be represented by the principle of virtual velocities:

$$P\dot{\delta} = \dot{E}_b + \dot{E}_m. \tag{26}$$

Using eqns (8), (5), (18), (24) and (25), the normalized instantaneous crushing force in the first half of the cycle can be recast in the form:

$$\frac{P(\alpha)}{P_m} = f_1(\alpha, m) + f_2(\alpha, m), \tag{27}$$

where the functions f_1 and f_2 are defined in Appendix A. In the second half of the cycle the same formulae would apply with m replaced by $(1-m)$. Of particular interest are peak values of the crushing force which occur at the instant of touching, i.e. where $\cos\alpha = \cos\alpha_0 = m$ and $\cos\alpha = 1-m$. Equation (27) is then reduced to

$$\frac{P}{P_m} = \frac{1+\sqrt{1-m^2}}{\pi m} + \frac{\sqrt{1-m^2}}{m} \tag{28}$$

for the first peak. The subsequent peak is obtained by replacing m with $(1-m)$. In the case of symmetric folding $m = 0.5$ and the normalized first and second peaks are of the same magnitude:

$$\frac{P}{P_m} = 2.92. \tag{29}$$

This so-called "corner load" is usually smaller than the initial peak load of the cylindrical shell. For an eccentric folding with $m = 0.25$ or $m = 0.75$, the normalized force alternates between two corner values:

$$\frac{P}{P_m} = 6.37 \quad \text{and} \quad \frac{P}{P_m} = 1.59. \tag{30}$$

A minimum value of the instantaneous force is reached just before touching, i.e. when $\alpha = 0$. From eqns (27) and (A1) the normalized minimum crushing force is

$$\left(\frac{P}{P_m}\right)_{min} = \frac{1}{\pi} = 0.31. \tag{31}$$

A sketch of the load–deflection relationship for the two cases discussed above is shown in Fig. 7. After a corner load is reached, the crushing force decreases monotonically to the minimum value until the next touching occurs, and so on.

Also shown in Fig. 7 is the load–deflection relationship for $m = 0$ which is the special case corresponding to the Alexander model. It can be observed from Fig. 7 that the present model with a non-zero value of the eccentricity parameter m predicts twice the number of peaks when compared to the Alexander model or any other model proposed to date (for the same crush distance). The presence of intermediate peaks is confirmed by experimental observation (see Fig. 1).

The present model with finite alternating peaks is certainly much better than any other model proposed to date. However, the effective crush distance, the average crushing force and the shape of the curved crushed lobes are not satisfactorily captured in the above simple model. Also, the stiffening phase near the touching point is too abrupt.

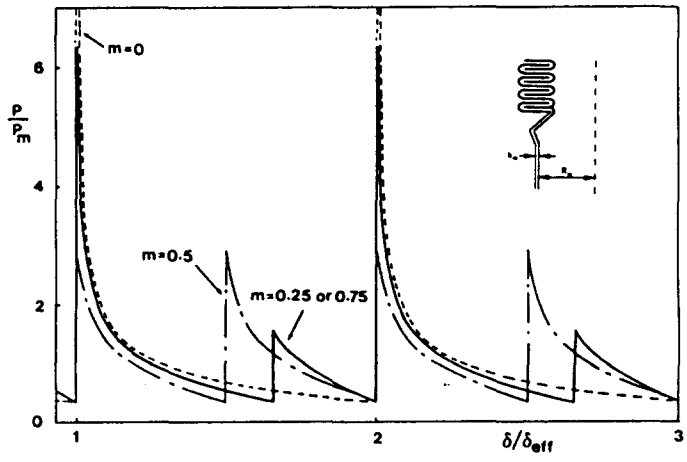

Fig. 7. A load–displacement diagram of a straight-element model for three values of the eccentricity parameter.

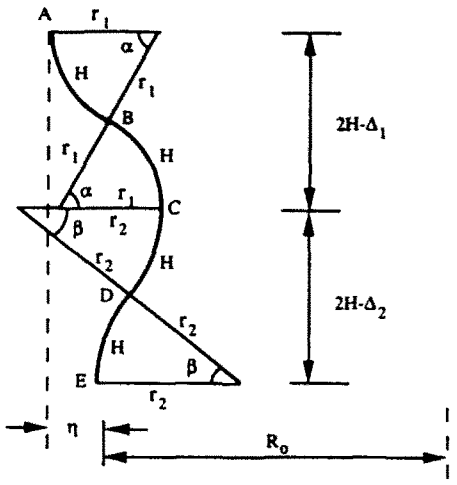

Fig. 8. A geometry of the transition zone with two curved superfolding elements.

5. MODEL WITH CONTINUOUS DEFORMATIONS

More accurate predictions of the mean crushing force, the length of the folding wave and the effective crush distance will be obtained by considering the model of the transition zone, consisting of two "S" shape SEs, introduced in Section 3. The concept of the folding of two curved elements is the same as in the previously considered case with straight elements. However, the geometry of the problem is far more complex. Therefore, only the main results are stated and the bulk of calculations is moved to Appendix B.

Geometry

An instantaneous geometry of the transition zone is shown in Fig. 8. The shape and instantaneous position of the SE is uniquely determined by the instantaneous radii r_1, r_2 or angles α and β:

$$r_1 = \frac{H}{\alpha}, \quad r_2 = \frac{H}{\beta}.$$

Furthermore, for a given eccentricity η, or the dimensionless eccentricity parameter m, the angles α and β are uniquely related:

$$\eta = \frac{2H}{\alpha}(1-\cos\alpha) - \frac{2H}{\beta}(1-\cos\beta), \tag{32}$$

similarly to the previously considered case. The dimensionless parameter m is defined by

$$\eta = m(R_{out} - R_{in}), \tag{33}$$

where R_{out} and R_{in} are defined in Fig. 9 showing one fully collapsed SE of length $2H$. From Fig. 9 one can calculate

$$\alpha_f = \frac{5\pi}{6},$$

$$r_f = \frac{H}{\alpha_f},$$

$$R_{out} - R_{in} = 2r_f\left(1 + \frac{\sqrt{3}}{2}\right). \tag{34}$$

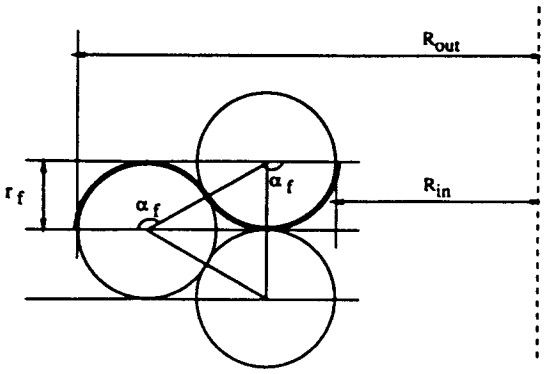

Fig. 9. Parameters, defining a fully crushed superfolding element.

Using eqns (33) and (34) the relation between α and β can be expressed in terms of the dimensionless eccentricity parameter m:

$$3m\frac{2+\sqrt{3}}{5\pi}-\frac{1-\cos\alpha}{\alpha}+\frac{1-\cos\beta}{\beta}=0. \tag{35}$$

A relation between the rates of the angles is obtained by differentiating eqn (36) with respect to time (see Appendix B). In order to calculate bending and membrane energies, it is necessary to determine the limits of variation of the angles α and β over the full folding cycle. These limits are:

$$\begin{aligned}\alpha_{\min}\leqslant\alpha\leqslant\alpha_f,\\ 0\leqslant\beta\leqslant\beta_f,\end{aligned} \tag{36}$$

where

$$\alpha_{\min}(m)=\beta_f(1-m). \tag{37}$$

The relationship between the maximum values of angles is obtained from eqn (35) by setting $\alpha=\alpha_f=5\pi/6$ and $\beta=\beta_f$. The calculated values of β_f for three different eccentricity parameters are given in the table below:

m	0.25	0.50	0.75
β_f	1.209	0.747	0.360

Finally, the shortening of the column at any value of the process parameter, α, is

$$\delta=\delta_1+\delta_2=2H\left[2-\frac{\sin\alpha}{\alpha}-\frac{\sin\beta}{\beta}\right]. \tag{38}$$

An expression for the rate of change of δ, $\dot{\delta}$, is given in Appendix B. The effective crush distance is defined as $\delta_{\text{eff}}=\delta_f-\delta_{\text{ini}}$ over the complete cycle, i.e.

$$\delta_{\text{eff}}=(\delta_f-\delta_{\text{ini}})_m+(\delta_f-\delta_{\text{ini}})_{1-m}. \tag{39}$$

It can be shown that in the case of symmetric folding, $m=0.5$:

$$\frac{\delta_{\mathrm{eff}}}{4H} = 1 - \frac{3}{5\pi} = 0.81. \tag{40}$$

The above results can also be obtained in a more straightforward manner by considering the geometry of the fully crushed column, to be represented by a system of densely packed alternating circles (Wierzbicki, 1990).

Bending energy

The SEs in the transition zone undergo continuous bending with a curvature $K = 1/r$ increasing from zero to the final value $K_f = 1/r_f$. The rate of bending energy is defined as

$$\dot{E}_b = \int_{ABCDE} |M_0 \dot{K}| 2\pi R_0 \, ds, \tag{41}$$

where the rate of curvature of the "S" elements are:

$$\text{Element ABC} \quad \dot{K} = -\frac{\dot{r}_1}{r_1^2} = \frac{\dot{\alpha}}{H},$$

$$\text{Element CDE} \quad \dot{K} = -\frac{\dot{r}_2}{r_2^2} = \frac{\dot{\beta}}{H}. \tag{42}$$

Because the curvature rate is constant along each element, the integration in eqn (41) can be readily performed to give

$$\dot{E}_b = 4\pi R_0 M_0 (|\dot{\alpha}| + |\dot{\beta}|) = 4\pi R_0 M_0 \dot{E}_b, \tag{43}$$

where E_b is a dimensionless bending rate of energy. Note a similarity between the above expression and the corresponding formula derived for the simplified model [eqn (8)].

Membrane energy

The membrane energy is defined by eqn (14), where the hoop strain rate is defined as

$$\dot{\varepsilon}_{00} = \frac{\dot{R}}{R_0}. \tag{44}$$

The expressions for $\dot{R}$ are different for each half of the SE and are given in Appendix B. Here R denotes the current position of a material point in the transition zone from the axis of the tube. The total rate of membrane energy can be represented in the form

$$\dot{E}_m = 2\pi\sigma_0 h H^2 \dot{\bar{E}}_m, \tag{45}$$

where the dimensionless rate of the membrane energy $\dot{E}_m$ is calculated in Appendix B. Now, the instantaneous crushing force can be calculated from eqn (26). Substituting the equations for $\dot{\delta}$, $\dot{\bar{E}}_b$ and $\dot{\bar{E}}_m$, the expression for the normalized crushing force takes the form:

$$\frac{P}{M_0} = p_1(\alpha)\frac{H}{R_0}\frac{2R_0}{h} + p_2(\alpha)\frac{R_0}{H}, \tag{46}$$

where the functions p_1 and p_2 are defined in Appendix B. The above solution involves a still unknown length of the folding wave H. As in the previously considered model, the unknown H will be determined from the minimum condition

$$\frac{dP_m}{dH} = 0, \tag{47}$$

where

$$P_m = \frac{1}{\delta_{eff}} \int_{ABCDE} P\delta \, d\alpha. \tag{48}$$

Substituting eqn (40) into eqn (48), the formula for the normalized mean crushing force can be recast into the form

$$\frac{P_m}{M_0} = P_1 \frac{2R_0}{h} \frac{H}{R_0} + P_2 \frac{R_0}{H}, \tag{49}$$

where the coefficients P_1 and P_2, defined in Appendix B, do not depend on the eccentricity parameter m.

The formula for the wavelength, calculated for the optimality condition is

$$\frac{H}{R_0} = \sqrt{\frac{h}{2R_0}} \sqrt{\frac{P_2}{P_1}}. \tag{50}$$

Substituting eqn (50) into eqn (49), the expression for the mean crushing force becomes

$$\frac{P_m}{M_0} = 2\sqrt{\frac{2R_0}{h}} \sqrt{P_1 P_2}. \tag{51}$$

A small computer program was written to calculate the coefficients in the above two expressions and the results are:

$$\frac{H}{R_0} = 1.31\sqrt{\frac{h}{2R_0}}, \tag{52}$$

$$\frac{P_m}{R_0} = 31.74\sqrt{\frac{2R_0}{h}}. \tag{53}$$

Substituting eqns (50) and (51) into eqn (46), the final expression for the instantaneous crushing force, normalized with respect to the mean crushing force, takes the form:

$$\frac{P(\alpha)}{P_m} = \frac{1}{2}\frac{p_1(\alpha)}{P_1} + \frac{1}{2}\frac{p_2(\alpha)}{P_2}. \tag{54}$$

Therefore, the dimensionless force history in the present solution is independent of the radius to thickness ratio of the shell and depends only on the eccentricity parameter.

6. DISCUSSION AND COMPARISON WITH EXPERIMENTS

Apart from numerical coefficients, the solution for H/R_0 and P_m/M_0 for the models with straight and curved lobes is similar. The magnitude of the coefficients is approximately 40% higher in the solution with curved lobes, which corresponds more closely to reality. A comparison of the theoretical mean crushing force [eqn (53)] with experimental data for

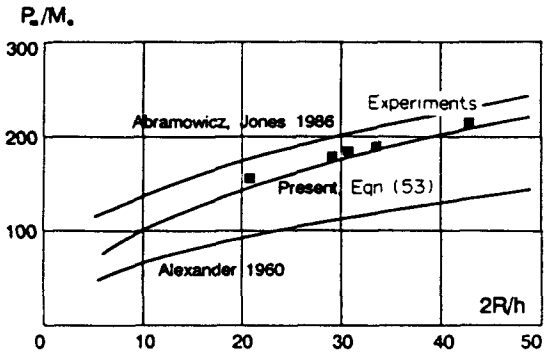

Fig. 10. Comparison of experimentally measured mean crushing force with prediction of various theories.

mild steel tubes (Abramowicz, 1990) is presented in Fig. 10 showing very good agreement. In bringing the experimentally measured force to the dimensionless form, the flow stress σ_0 *was assumed to be equal to 92% of the ultimate stress* of the material. This was obtained by calculating the mean stress in the strain range of interest.

The force history for three values of the eccentricity parameter $m = 0.25, 0.5, 0.75$ is plotted in Fig. 11 taking as an independent variable the normalized axial shortening of the tubes. Compared to the solution based on the simplified model, two features should be pointed out. The stiffening phase is now more gradual. The total loading cycle is shorter and equal to $\delta_{\text{eff}} = 0.81(4H)$ rather than $4H$. Also, the position of the intermediate peak shifts, depending on m. In the case $m = 0.5$, the folding is symmetric in the sense that all peaks are equal in magnitude and equally distanced from each other. For $m = 0.25$, or $m = 0.75$, the distances between subsequent peaks alternate even though the lengths of two SEs in the active transition zones are the same. An experimental force–deflection curve confirms all of the above features of the present theoretical solution (see Fig. 1). The dimensionless crushing force fluctuates between the extreme values $0.45 \leqslant P/P_m \leqslant 3.1$ in the case of symmetric folding. In the simpler, linear model, the variation was in the range $0.31 \leqslant P/P_m \leqslant 2.92$. Unsymmetric folding, corresponding to $m = 0.25$ exhibits a rather large spread in the alternating peak loads 1.71–6.74. Such a large difference is not observed experimentally. This discrepancy can be attributed to a number of factors. First, the work hardening of the material as well as lateral crushing of the newly-formed lobe will smooth out a transition from the stiffening to the softening phase. Secondly, there will be some out-of-plane deformation of the shell caused by initial elastic–plastic buckling so that progressive folding proceeds in an imperfect shell. Finally, three or even four active folding elements could form a transition zone and the resulting deformation could reduce sharp force spikes.

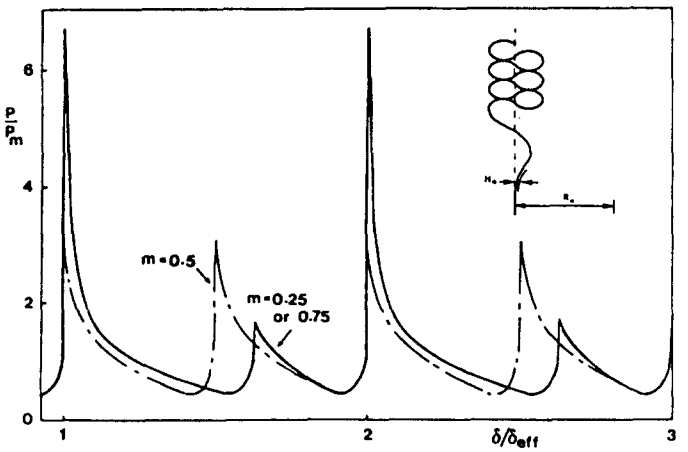

Fig. 11. Force–displacement history of a curved element model. Note a gradual stiffening phase and unequal magnitude and position of subsequent peaks.

Note that a cut-off value at a squash load has not been introduced in Fig. 11. The squash load is understood as the yield stress times the cross-sectional area.

The only feature of the solution that cannot be predicted by the present computational model is the amount of eccentricity. Experimental observation suggests that relatively thick tubes fold more outside their initial radius than inside (Grzebieta and Murray, 1989). At the same time thinner cylinders as well as prismatic columns fold in a more or less symmetric fashion. The fact that the mean crushing force does not depend on the eccentricity parameters suggests that the dependence of the load history on m should be rather weak. Therefore, a collection of second order effects could be responsible for any specific folding pattern. One important factor is the definition of hoop strain and strain rate. In eqn (44) an engineering definition was adopted for simplicity. In a more rigorous approach, the velocity $\dot{R}$ should be referred to the current thin initial tube radius

$$\dot{\varepsilon}_{\theta\theta} = \frac{\dot{R}}{R}. \tag{55}$$

According to eqn (55), folding "in" ($R < R_0$) would produce larger strain rates than folding "out" ($R > R_0$). Also, large strains present in the present problems will produce a large thickness variation. Inside lobes, subjected to compression, will be appeciably thicker than outside lobes that are subjected to tension. Accordingly, the bending resistance of outer and inner lobes would differ favoring predominantly outside folding. Also, the finite thickness of the shell was not included in building up the geometry of the problem and establishing conditions for touching. The latter effect could be incorporated relatively easily into the theory (Wierzbicki and Bhat, 1986), while two former ones will complicate the mathematics rendering it analytically untractable.

7. EFFECT OF STRAIN REVERSAL AND STRAIN-HARDENING

An interesting property of the phenomenon of progressive folding is that any material point of the shell undergoes a complex loading history involving tension and compression. The effect of strain reversal is thus accounted for by the present theory. We shall explain it using the model with stationary hinges. Consider the material point such as B in Fig. 6. This point has already moved inside the tube and has undergone a certain amount of compressive plastic strain. As a new folding cycle starts at $\alpha = \alpha_0$ in Fig. 6, the point B travels outside, across the original tube radius, and settles down at its final location outside the tube radius R_0. Corresponding stress trajectories of the point B in the present rigid-plastic material idealization and also for a more realistic strain hardening material are drawn in Fig. 12. It is difficult to take into account the effect of strain-hardening in a rigorous way in the present computational model. It is recognized that this effect will change (generally smooth out) the load-deflection history and introduce a small correction to the value of the mean crushing force. In the present theory the effect of work-hardening is accounted for in an approximate manner through the constant but elevated magnitude of the flow stress σ_0. The flow stress can be related to the average magnitude of the strain

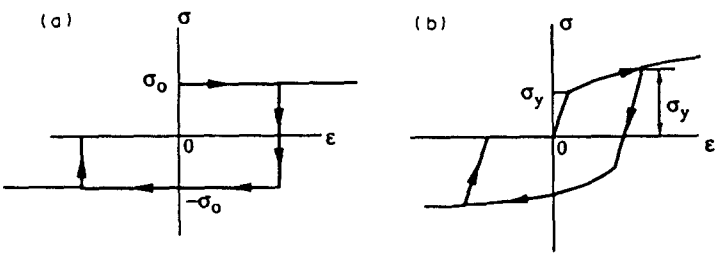

Fig. 12. A typical loading path of a material point of a cylinder in (a) a rigid-perfectly plastic material and (b) an elastic-plastic work-hardening material.

attained in the inside or outside lobes. In the case of symmetric folding with $m = 0.5$, the average hoop strain equals

$$\varepsilon_{av} = \frac{H}{2R_0} = 0.443\sqrt{\frac{h}{2R_0}}. \tag{56}$$

For example, in a thick tube with $R_0/h = 10$, the average compressive or tensile strain reaches 10%.

The effect of strain reversal has not been predicted in any of the existing models of progressive crushing of tubes.

8. INITIATION OF THE FOLDING PROCESS

The formation of the first few folds in the undeformed tube requires a separate consideration. A simplified model with straight elements will suffice for explaining the concept if the edge of the tube is prevented from sliding, for example by friction, then the geometrically compatible model of the transition zone should consist of three segments, as shown in Fig. 13. Because the first lobe usually forms outside, the length of the additional segment is taken to be $2H(1-m)$. In general, the three-segment model represents a two-degrees-of-freedom system. It is reasonable to assume that the first two segments are inclined by the same angle to the horizontal line. It is straightforward to derive formulae for the instantaneous crushing force, following the procedure explained in Section 4. The force-deflection relation will start at infinity and gradually diminish until first contact occurs at a crush distance equal to $\delta_f = 2H(2-m)$. *Thus, in symmetric folding the distance between the first two peaks is equal to* $3H$. Subsequent peaks are positioned at $2H$ intervals. Again, the above theoretical result is fully confirmed by experiments on circular tubes and multi-cornered prismatic columns.

The magnitude of the first peak is governed by elastic-plastic shell buckling and must be determined from separate considerations.

9. CONCLUSIONS

A new model of the progressive crushing of tubes was developed in which the active zone of plastic deformation contains two Superfolding Elements. The deformation process of each material point within the shell is characterized by strain reversal. The new model captures with great realism several effects unaccounted for in all previous analytical models of plastic folding. These include description of a softening, followed by a stiffening phase,

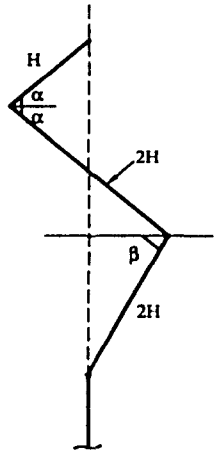

Fig. 13. A three-element model of the initiation of the folding process.

alternating lower and higher peaks, unequal distance between subsequent peaks, and a reduced crush distance.

Accurate formulae were also derived for the optimum length of the plastic folding wave and the mean crushing force, in terms of a radius to thickness parameter and an average flow stress of the material. The validity of these formulae was checked against experimental data over a range of radius to thickness ratios showing a very good agreement. The influence of other effects such as work hardening of the material, thickness variation and alternative definition of the hoop strain rate were also discussed.

The history of the crushing force was calculated over a full deformation cycle. It was shown that the plot of the crushing force, normalized with respect to the mean crushing force is independent of the geometrical parameters of the shell and depends only on the eccentricity parameter.

The present concept of folding over two active elements can be easily extended to cover multi-corner prismatic columns. A geometry of the transition zone of such columns has already been constructed as depicted in Fig. 14 showing subsequent deformation states of the two-element model (compare with Fig. 5). The necessary calculations will be performed in a future continuation of this research.

Acknowledgement—The work reported herein was sponsored, in part, by the M.I.T.—Industry Crashworthiness Consortium.

REFERENCES

Abramowicz, W. (1990). Personal communication.

Abramowicz, W. and Jones, N. (1986). Dynamic progressive buckling of circular and square tubes. *Int. J. Impact Engineering* **4**(4), 243–269.

Abramowicz, W. and Wierzbicki, T. (1989). Axial crushing of multi-corner sheet metal columns. *J. Appl. Mech.* **56**, 113–120.

Alexander, J. M. (1960). An approximate analysis of the collapse of thin cylindrical shells under axial loading. *Q. J. Mech. Appl. Math.* **13**(1), 10–15.

Brodkin, D. (1988). Modelling the progressive crushing of shell structures using computer graphics. M.S. Thesis, Dept. Civil Engineering, Massachusetts Institute of Technology.

Grzebieta, R. H. and Murray, N. W. (1989). Rigid plastic collapse behavior of an axially crushed stocky tube. *Proc. ASME Winter Annual Meeting*, Dec. 10–15, San Francisco, AMD-Vol. 105.

Hallquist, L. and Benson, D. (1986). Dyna 3D, a computer code for crashworthiness engineering. *Proc. of International FEM Congress*, Baden-Baden, Germany, Nov. 17–18, pp. 169–188.

Haug, E. *et al.* (1986). Numerical techniques, experimental validation of structural impact and crashworthiness analysis with supercomputers for the automotive industry. *Proc. of the International Conference on Supercomputer Applications in the Automotive Industry*, Switzerland (organized by Cray Research Inc., Edited by C. Marino). A *Computational Mechanics* Publication, pp. 127–146.

Johnson, W., Soden, P. and Al-Hassani, S. T. S. (1977). Inextensional collapse of thin-walled tubes under axial compression. *J. Strain Anal.* **12**, 330–337.

Jones, N. (1989). *Structural Impact*. Cambridge University Press, Cambridge.

Magee, C. L. and Thornton, P. H. (1978). Design consideration in energy absorption by structural collapse, SAE Paper # 780434. *Proc. Congress and Exposition*, Cobo Hall, Detroit, Feb. 27–March 3.

Mahmood, H. F., Paluszny, A. and Tang, X. D. (1986). A 3-D computer program for crashworthiness analysis of vehicle structure composed of thin-walled beam components. *Proc. ASME Winter Annual Meeting*, Anaheim, California, Dec. 7–12, AMD-ref. 79.

Pugsley, A. G. (1979). On the crumpling of thin tubular struts. *Q. J. Mech. Appl. Math.* **32**, 1–7.

Pugsley, A. G. and Macaulay, M. (1960). The large scale crumpling of thin cylindrical columns. *Q. J. Mech. Appl. Math.* **13**, 1–9.

Soden, P. D., Al-Hassani, S. T. S. and Johnson, W. (1974). The crumpling of polyvinylchloride tubes under static and dynamic axial loads. Inst. Physics Conference Ser., No. 21, pp. 327–338.

Wierzbicki, T. (1990). Plastic folding wave and effective crash distance. *Impact Design*, No. 1.

Wierzbicki, T. and Bhat, S. (1986). A moving hinge solution for axisymmetric crushing of tubes. *Int. J. Mech. Sci.* **28**(3), 135–151.

APPENDIX A

The expressions for $w(s)$ and $\dot{w}(s)$ in the deforming regions are given by

$$\left.\begin{aligned} w(s) &= s\cos\alpha - 2H\cos\alpha_0 \\ \dot{w}(s) &= -s\sin\alpha\,\dot{\alpha} \end{aligned}\right\}\ldots\text{on AC},$$

$$\left.\begin{aligned} w(s) &= s\cos\beta \\ \dot{w}(s) &= -s\sin\alpha\,\dot{\alpha} \end{aligned}\right\}\ldots\text{on CD}. \tag{A1}$$

The functions entering the right-hand side of eqn (27) are

$$f_1 = \frac{1}{\pi}\frac{1+\dfrac{\sin\alpha}{\sqrt{1-(\cos\alpha-m)^2}}}{\cos\alpha+\dfrac{\sin\alpha(\cos\alpha-m)}{\sqrt{1-(\cos\alpha-m)^2}}},$$

$$f_2 = \frac{\sin\alpha}{\cos\alpha+\dfrac{\sin\alpha(\cos\alpha-m)}{\sqrt{1-(\cos\alpha-m)^2}}}. \tag{A2}$$

APPENDIX B

$$\beta = \frac{\dfrac{\sin\alpha}{\alpha}-\dfrac{1-\cos\alpha}{\alpha^2}}{\dfrac{\sin\beta}{\beta}-\dfrac{1-\cos\beta}{\beta^2}}\dot{\alpha},$$

$$\dot{\overline{E_M}} = \int_{ABC}\left|\frac{\dot{R}}{H^2}\right| r_1\,\mathrm{d}\phi + \int_{CDE}\left|\frac{\dot{R}}{H^2}\right| r_2\,\mathrm{d}\phi,$$

where ϕ is a current angular coordinate of a generic point on the arc ABCD, measured from the horizontal position:

$$\dot{\delta} = \frac{\dot{\alpha}}{\alpha^2}[\alpha\cos\alpha-\sin\alpha]-\frac{\dot{\beta}}{\beta^2}[\beta\cos\beta-\sin\beta], \tag{B1}$$

on AB

$$\dot{R} = -\frac{H}{\alpha^2}\dot{\alpha}\{\phi\sin\phi-1+\cos\phi\}, \tag{B2}$$

on BC

$$\dot{R} = -\frac{H\dot{\alpha}}{\alpha^2}[1-2\cos\alpha+\cos\phi-2\alpha\sin\alpha+\phi\sin\phi], \tag{B3}$$

on CD

$$\dot{R} = -\frac{H\dot{\beta}}{\beta^2}[1-2\cos\beta+\cos\phi-2\beta\sin\beta+\phi\sin\phi], \tag{B4}$$

on DE

$$\dot{R} = -\frac{H}{\beta^2}\dot{\beta}\{\phi\sin\phi-1+\cos\phi\}, \tag{B5}$$

$$\dot{\overline{E_b}} = |\dot{\alpha}|+|\dot{\beta}|, \tag{B6}$$

$$\dot{\overline{E_m}} = \int_{AB}\left|\frac{\dot{R}}{H^2}\right| r_1\,\mathrm{d}\phi + \int_{BC}\left|\frac{\dot{R}}{H^2}\right| r_1\,\mathrm{d}\phi + \int_{CD}\left|\frac{\dot{R}}{H^2}\right| r_2\,\mathrm{d}\phi + \int_{DE}\left|\frac{\dot{R}}{H^2}\right| r_2\,\mathrm{d}\phi, \tag{B7}$$

$$p_1(\alpha) = 2\pi\frac{\dot{\overline{E_m}}}{\dot{\delta}}, \tag{B8}$$

$$p_2(\alpha) = 2\pi\frac{\dot{\overline{E_b}}}{\dot{\delta}}, \tag{B9}$$

$$P_1 = \frac{1}{\dot{\delta}_{\mathrm{eff}}}\left\{\int_{\alpha_{\min}(m)}^{\alpha_f(m)} p_1\dot{\delta}\,\mathrm{d}\alpha + \int_{\alpha_{\min}(1-m)}^{\alpha_f(m)} p_1\dot{\delta}\,\mathrm{d}\alpha\right\}, \tag{B10}$$

$$P_2 = \frac{1}{\dot{\delta}_{\mathrm{eff}}}\left\{\int_{\alpha_{\min}(m)}^{\alpha_f(m)} p_2\dot{\delta}\,\mathrm{d}\alpha + \int_{\alpha_{\min}(1-m)}^{\alpha_f(m)} p_2\dot{\delta}\,\mathrm{d}\alpha\right\}. \tag{B11}$$

$$\frac{2H}{}$$